AIAA-2001-0310

Wind Tunnel Testing of the Wright Brothers Model B Airfoil

Drew Landman*, Julian Alvarez†, Spiros Blackburn†, and Robert Ash‡
Department of Aerospace Engineering
Old Dominion University, Norfolk, VA
Ken Hyde
The Wright Experience, Warrenton, VA

Abstract

Wind tunnel tests of a Wright Model B airfoil have been conducted using two-dimensional models in full and third-scale at flight Reynolds numbers. In an effort to ascertain the effect of rib and covering construction on airfoil aerodynamics, the full-scale model was fabric covered and maintained the original dimensions of the Wright Model B Flyer wing. Since the full-scale model could only be tested over a small angle-of-attack range, a solid surface, third-scale pressure model was constructed. Lift and pitching moment polars from the tests are presented over a range of angles-of-attack spanning zero-lift to post stall. A drag polar is presented for an angle-of-attack range from -4 to 6 degrees. Surface static pressure distributions are presented from the third-scale model. Flow visualization study results are presented from surface mounted tufts on both models and are used to corroborate force and pressure data findings.

Background

The Wright Experience, Old Dominion University (ODU), Wichita State University and NASA Langley Research Center (LaRC) sponsored two wind tunnel tests on a Wright Model B airfoil geometry. The Model B, the first production Wright aircraft, has the most complete engineering specifications and documentation available and was chosen as the first test article in a planned series of tests to evaluate the performance of early Wright aircraft. Ken Hyde of the Wright Experience plans to fly the Model B, following wind tunnel testing, in an effort to better understand handling qualities and familiarize himself with the unique controls. The overall test program, aimed at eventually flying a true 1903 reproduction, will proceed by moving back in time from the 1910 Model B Flyer to test the 1905 and finally the 1903 Flyers. Propeller tests and now airfoil tests have been completed on the Model B, while a full-scale aircraft test is slated for the ODU Langley Full-Scale Tunnel in the summer of 2001. The Wright Experience has been chosen by the Experimental Aircraft Association to build the National Park Service's 1903 flight worthy, exact reproduction for the centennial celebration of the Wright's first flight at Kitty Hawk, NC.

This paper presents wind tunnel test results from full-scale and third-scale two-dimensional airfoil tests conducted at the National Institute for Aviation Research (NIAR) and NASA Langley Research Center respectively. It is hoped that the data from this test will benefit not only the current program but also provide a historically significant database for Wright airfoils.

Introduction

The Model B flyer, first produced in 1910, is shown in figure 1. This biplane had an overall length of 28 feet and a gross weight of 1250 lbs. The wing spanned 39 feet with a chord of 74 inches, camber of 1/20 and wing area of 500 square feet.[1] Propulsion was provided by a single 39 horsepower engine that drove two counter rotating pusher propellers through a chain drive.[2] Control was through dual levers that moved fore and aft. One lever provided pitch control through a full flying stabilizer and the other coupled roll and yaw control through wing warping and a full flying rudder.[3] In addition, a small secondary stick on the lateral control stick allowed trimming the rudder in turns.

While the airfoil geometry looks similar to the 1903 Wright Flyer, they are quite different. The leading edge radii are identical, but the 1903 airfoil thickness tapers continuously along the chord line where the Model B is constant thickness, until the trailing spar where it then tapers to the trailing edge. The Model B wing design is consistent with the 1903 in that the load is carried by the leading edge spar and a trailing spar, as shown in

* Assistant Professor, Member AIAA,
† Graduate Research Assistant, Student Member AIAA
‡ Eminent Scholar, Member AIAA

the plan view of figure 2. The covering on the Model B is attached to the bottom surface of the ribs via a pocket sewn into the fabric; the top surface fabric was *not* attached to the ribs, but only to the leading edge spar and to a trailing edge wire. The hardened steel wire was encased in a pocket sewn into the trailing edge of the fabric covering which was pulled tight to give the scalloped appearance in the wing plan view. The rib design consists of two cap strips and various spacing blocks as shown in the end view of figure 3. The camber is 1/20 and the camber line follows an approximate circular arc.

Test Philosophy

The unique wing covering arrangement suggested a need for full-scale modeling of the airfoil to capture the aerodynamic effects of the suspected top surface fabric deformation. In particular, the fabric effect on minimum drag and cruise lift coefficient were of great interest to planned aircraft performance simulations. Unfortunately, the size of the chord prohibited full-scale testing of the airfoil in traditional two-dimensional airfoil testing facilities. A search for available facilities with adequate 2-D test section areas to allow a full angle-of-attack sweep without excess blockage proved unsuccessful. Since the project budget fell short of constructing a 2-D insert for existing large scale facilities, it was decided to proceed with this test in two phases. A full-scale model was constructed for use in a 7 X 10 foot test section restricted to a limited angle-of-attack sweep. A second model was constructed at one third-scale for use in a traditional 2-D airfoil test facility. In this manner, the effects of the fabric could be ascertained for the typical operating range of the aircraft and compared to the complete polar of the third-scale model.

The Walter H. Beech Memorial 7 X 10 Foot Low Speed Wind Tunnel at Wichita State University (WSU 7 x 10) was used for full-scale testing. A floor to ceiling model was constructed to span the 7 foot test height of this 7 X 10 foot test section. Lift data was obtained with the floor to ceiling force balance and drag data using a wake rake. The NASA LaRC Low Turbulence Pressure Tunnel (LTPT) was chosen for the excellent flow quality and ability to pressurize the test section to achieve flight Reynolds numbers with a relatively inexpensive model structural requirement. Lift and pitching moment data was obtained using surface pressures and drag with a wake rake. Flow visualization was conducted using wool tufts in both facilities. Both airfoil models were designed to be tested at the cruise flight Reynolds number of 2.6 million.

Airfoil Models

Historical Data and Computational Model

A literature search for existing data on any Wright airfoil was conducted with controversial results since the references did not clearly identify the airfoil geometry (or in some cases test conditions). Since there was a certain lack of confidence concerning load prediction, and no published pressure distributions (to better place model pressure orifices), a 2-D computational model was attempted using smoothed measured coordinates from a reproduction rib with Airfoil II™ and Xfoil™. The computational Model B geometry had to be modified for code convergence due to the unusually blunt leading edge and thick trailing edge. The original and modified geometry used with a successful Airfoil II ™ run are shown in figure 4. The lift polar from the Airfoil II™ model using the flight Reynolds number of 2.6 million is included with the available reference data in figure 5. The "deep stall" portion of the curve is an artifact of this coupled boundary layer-inviscid flow method which was never intended to model the large scale separation which occurs on the Wright airfoils. The curves labeled Wright No. 12 and 18 are data from the Wright Brother's original notes published in McFarland.[4] Comparison of the measured full-scale ribs show that the camber line of the Model B most closely resembles the No. 18 geometry. These models were made of sheet metal plates of constant thickness with a maximum camber of 1/20. The data comes from the Wright's 1901 wind tunnel test, performed at a fixed Reynolds's number of 58,000. The data noted as Eiffel 10 in figure 5 was taken at the Eiffel Laboratory at a Reynolds number of 103,000 in 1913 and published by the NACA in 1921, labeled as a Wright profile.[5,6] The curve labeled Loukianoff is from Von Mises' *Theory of Flight* which in turn cites his source as the work of Loukianoff.[7,8] At the time of this writing, it was not possible to obtain a copy of this 1912 German publication in order to identify the test conditions. Differences in the reference data, particularly the maximum lift coefficient is most likely due to extensive laminar separation on the low Reynolds number models.[9] Comparison of available drag data, as might be expected, contained even more scatter. For the model structural design purposes of this study, a maximum lift coefficient of approximately 1.4 was chosen as a safe maximum. A sample pressure distribution from the computational model is shown in figure 6 and reveals characteristic leading edge peaks on the top and bottom surface and the relatively constant pressure regions from x/c = 0.20 to the trailing edge.

Full-Scale

The balance system of the NIAR 7 x 10 relies on a rigid model design to insure accurate in situ calibration. To this end, a steel spar structure with aluminum ribs was designed for minimum model deflection. Model B rib reproduction tooling was created by The Wright Experience to manufacture the wing. Coordinates for the rib jigs were obtained by measuring ribs from a surviving Wright Model B wing panel and an isolated rib from a second source. A newly manufactured reproduction rib was then measured using a coordinate measuring machine and the data set used to produce tool paths for computer numerical controlled (CNC) milling of the ribs. The reinforced design maintained the geometry of the original covered wing, with the exception of rib spacing at the ends. The covering material was the identical material used on the 1910 aircraft, a rubberized cotton, and it was attached to the ribs in the same manner as the original.[10] The wooden leading edge was reproduced in order to allow nailing of the top surface covering material. Fabric rib pockets were used on the lower surface and a trailing edge wire secured the trailing edge fabric. The model is shown in figures 7 and 8.

Third-Scale

The third-scale model was of composite design utilizing a steel main and auxiliary spar system, aluminum end ribs, a structural foam core and a fiberglass and epoxy resin covering. The model ribs and spars with the foam removed are shown in figure 10. Mounting tangs were attached to the end ribs for use in the LTPT. The aluminum ribs were computer numerical machined using the scaled geometry from the full-scale model. The foam was rough cut and glued to the rib assembly using a mix of epoxy and fairing filler which was then carefully shaped to profile using a large sanding bar with the end ribs as guides. Pressure tubing channels for 31 surface orifices were routed into the foam core, glued, and filled (as shown in figure 10), before the fiberglass skin was applied with the vacuum bagging technique. Pressure orifices were then drilled into the surface of the model through to the underlying tubing.

Experimental Details

Angle-of-attack is referenced to a line of tangency on the airfoil bottom surface, found by positioning the model on a flat surface as shown in figure 3.

Full-Scale

The WSU 7 X 10 is a closed return, atmospheric pressure, closed throat, 7 X 10 foot rectangular test section low-speed wind tunnel. The large-scale two-dimensional airfoil balance system relies on strain gage load cell force measurements in both the floor and ceiling, spanning the 7-foot height. This system is capable of measuring lift, drag, and pitching moment. Test section calibrations for the dynamic pressure show a turbulence factor of approximately 1.4, buoyancy of -0.0055/ft (C_p/ft), and flow angularity of less than 0.1 degrees over the entire test section area.[11] In this experiment, the dynamic pressure was chosen based on the full-scale Reynolds number of 2.6 million and averaged approximately 6.6 psf. The relatively low forces at these conditions required the measurement of drag by wake survey, accomplished using a fixed rake of total pressure probes with tube spacing of 0.125 inches. The rake was constrained to operate at a distance of 44.5 inches downstream of the trailing edge. Pressures were measured using a PSI 8400 electronic pressure scanner with a range of 2.5 psid calibrated using a 1 psi range precision unit. Lift forces were sampled from the load cells using a HP 3852 data acquisition system. Tufts on both surfaces were filmed during the test with video recorders for posttest analysis.

A pretest evaluation of the boundary corrections incurred over an angle-of-attack sweep from -4 to 4 degrees, using the predicted forces and the method of reference 12, showed that it should be possible to measure the lift and drag coefficients with less than a 15% correction at the limits. The full-scale model installed in the test section of the WSU 7 X 10 with the drag rake is shown in figure 11.

Third-Scale

The LTPT is a pressurized, closed throat, 3 X 7.5-foot rectangular test section wind tunnel purposely designed for 2-D airfoil testing. A test section pressure of 4 atmospheres was selected in order to achieve a Reynolds number of 2.6 million while maintaining relatively small loads on the model. At this operating pressure the approximate Mach number and dynamic pressure were 0.048 and 13.7 psf respectively. Lift and pitching moment were evaluated by integrating surface pressures. The measurement of drag was again by wake survey, accomplished using a traversing rake of total pressure probes providing a reading every 0.10 inches. Pressures were measured using a PSI 8400 electronic pressure scanner with a range of 1 psid calibrated using a 1 psi range precision unit. More details concerning this historic facility can be found in reference 13. The third-scale model installed in the test section of the LTPT with the drag rake is shown in figure 9.

Results

Boundary corrections were applied to the force data of the full-scale test using the method described in reference 12. Wake blockage, solid blockage, streamline curvature and buoyancy were taken into account. Raw data from three angle-of-attack sweeps (runs) was combined and a least squares fit applied. The fitted raw data was then corrected and is shown in the plots at the corrected angles-of-attack. The limit to the angle-of-attack range was governed by the ability to obtain wake drag data. The wake size with respect to the rake limited the range (uncorrected angle-of-attack) to $-0.5° < \alpha < 3.5°$ which fell within the aforementioned limit of less than 15% correction to any value (C_l, C_d, C_m, α). Wake surveys from the full-scale test are shown in figure 13 plotted as wake position versus the ratio of dynamic pressure in the wake (q_w) to the freestream tunnel dynamic pressure (q_t). The $\alpha = -1°$ case illustrates a wake beyond the limits of the rake. The third-scale wake measurements were of similar shape for the corresponding angles-of-attack. The third-scale data is presented raw and uncorrected, the compilation of 6 runs. The third-scale test results are presented without correction for two reasons: 1) drag could be arguably only accurately measured by rake wake up to a maximum of $\alpha=6°$, but is required for the correction algorithm over the full pitch range, 2) the boundary corrections at the lower angles-of-attack were negligible.

Forces

The polars of figures 14-16 summarize the lift, drag, and pitching moment data from both tests. Correlation between the two models appears to be reasonable in all cases except the pitching moment. Note that there are fewer points shown for the third-scale drag results versus the lift and pitching moment. A portion of the drag data was eliminated due to equipment problems with the rake wake instrumentation. From the third-scale data, the maximum lift coefficient was found to be approximately 1.3 at an angle-of-attack of 9.5°. A minimum drag coefficient of about 0.010 was measured using the full-scale model whereas the third-scale model may show a slightly higher value. Of course these values have to be weighed with the uncertainty level of the test, presented in a later section. The zero-lift angle-of-attack occurs at approximately $\alpha = -4.0°$, the minimum drag at $\alpha = 1.6°$. The lift curve slope measured using the full-scale model is measurably steeper than the third-scale model and is thought to represent the influence of the fabric versus the solid surface model. The greatest difference between the two tests is seen in the pitching moment data of figure 15. The computational model results are plotted with the experimental results and seem to split the difference. It should be noted that the pitching moment data influences only the angle-of-attack in the correction algorithm. By varying the pitching moment between the third-scale values and the full-scale values and applying the boundary corrections, the corrected angle-of-attack was seen to vary by only 0.2°.

Pressure

Pressure data is presented in coefficient form for the 31 surface orifices. It should be noted that the aft most orifice was located in the relatively thick trailing edge. Figures 17 through 19 show representative pressure distributions from a single run as the model was pitched from zero lift through stall. No lift hysteresis was noted on returning the model to zero lift condition.

Flow Visualization

Woolen tufts were glued to the top and bottom surfaces of the full-scale model and videotaped through the tunnel ceiling and sidewall windows. Optical access to the third-scale model was limited to the airfoil top surface where linen thread tufts were attached and filmed. Table 1 summarizes the results from the surface flow visualization studies. The term reversal refers to tufts flowing in a direction opposite to the freestream flow direction that occurs for example in a recirculation bubble. Fluttering indicates motion of the tufts and when pronounced indicates large scale separation is present.

Experimental Uncertainty

The experimental uncertainty in the force and moment coefficients was calculated using the AIAA standard for wind tunnel data uncertainty and is summarized in table 2.[14] Precision was evaluated by repeated measurements and was calculated for a 95% confidence level. Bias was evaluated using existing facility instrument calibration data. The column labeled "N" in table 2 refers to the number of repeated measurements used to evaluate the precision and "U" is the overall uncertainty.

Discussion

The Model B airfoil may be described in modern terms as a high-lift section. The range of angle-of-attack over which the airfoil operates relatively efficiently is limited to 0-5°. This assertion is based first on the flow visualization studies which show measurable separation on either surface outside these limits. Beyond this, the pitching moment polar of figure 15 shows that the

aerodynamic center will start to move from the near quarter chord position, whereas the drag polar shows a marked rise in drag outside these pitch limits. To understand what flow phenomena define the limits of performance, it is necessary to correlate the force, pressure, and flow visualization study results.

Concerning the lower limit, the wake data of figure 13 reveals the lower surface separation witnessed in the flow visualization studies at low angles-of-attack. A recirculation bubble appears to form just aft of the leading edge and grows in size as the angle-of-attack is decreased from positive values. The influence of this bubble may be seen in the wake spreading of figure 13. The signature of this lower surface recirculation region may be seen in the pressure distribution of figure 17. At $\alpha = 0°$ the bubble influence is seen as a low pressure region near the leading edge. At $\alpha = -4°$ this low pressure region extends over most of the bottom surface. The pressure distributions explain the nonlinear behavior shown in the pitching moment polar (figure 15) at the negative angles-of-attack.[15,16]

The upper limit in angle-of-attack is governed by top surface separation. The extremely adverse pressure gradient resulting from the rather blunt leading edge geometry suggests a high probability of a laminar bubble followed by turbulent reattachment.[9,17] The tuft study supported this theory in that reversed flow was shown just aft of the leading edge for small positive angles-of-attack. Unfortunately, optical access at LTPT did not allow viewing of the leading edge beyond approximately $\alpha = 4°$. The pressure distributions of figures 18-19 appear to show the growing size of the leading edge separation bubble. For instance, consider the attenuated suction peak of $\alpha = 6°$ versus 4° and then the subsequent development of a constant pressure region over the first 10-15% of the top surface shown in the 8° case. The tuft study showed large-scale separation with flow reversal at the trailing edge for $\alpha = 10°$. This is supported by the pressure distribution at $\alpha = 12°$ showing the constant pressure region characteristic of a fully separated flow.

The effect of fabric deformation on airfoil performance within the normal operating range does not appear to be dramatic.[18] Lift and drag values obtained from the two different models correlate well and when considering the experimental uncertainty may be indistinguishable. One interesting observation was made when comparing the measured lift curve slope of the two tests. Clearly, the full-scale data indicates a higher value (of $dC_l/d\alpha$) over the measured range. Observations during full-scale tests revealed a slight "billowing" of the upper surface fabric particularly over the positive angle-of-attack range. One possible explanation is that as the loading increases over the top surface of the airfoil, the unsecured fabric assumes a slightly thicker and more highly cambered shape, gradually shifting the lift polar. By analogy, consider an airfoil with a plain flap and the hypothetical data of figure 20. The solid dark line represents the lift curve for the plain airfoil with zero flap deflection; the dashed lines, the lift curves for increasing values of flap deflection (increased camber).[19] If the flap were deflected incrementally as the angle-of-attack was increased, the effect would be to shift the lift curve slope to the thin solid line. A similar process may occur on the Model B airfoil as the fabric deflects under load to a greater camber with each increment in angle-of-attack.

The differences in the pitching moment results of the third-scale versus full-scale model have not been resolved. When comparing curve slopes, the trend is in the same direction for both wind tunnel tests and opposite the computational results. The argument used for the change in slope due to fabric deformation induced camber change would shift the slope in the opposite direction. The differences may be explained by a small spanwise deformation observed in the full-scale model or hysteresis in the balance system.

Conclusions

Wind tunnel tests on the Wright Model B Flyer airfoil have been conducted to document aerodynamic behavior. This airfoil test data will be added to the growing volume of information on this aircraft and used to help predict performance and handling characteristics. It is hoped that this test will not only help archive important engineering data on a historical aircraft but also help bring to life a flight worthy exact reproduction.

Acknowledgements

The authors would like to acknowledge the financial and technical support provided by NASA LaRC with special thanks to B. Crawford, J. Cruz, J. Kegelman, P. Phillips, F. Quinto, B. Sewall , and L. Yip. An equal debt of gratitude for financial and technical support is directed to Wichita State University, especially B. Johnson, S. Miller, and their students: G. Heim, G. Thumann and V. Tumwa. Thanks to M. Selig for consultation.

References

[1] Wald, Q.R., "Flying with The Wright Brothers, One Man's Experience," published by the Author, 1999

[2] Miley, S.J., Ash, R.L., Landman, D., Sparks, A.K., and Hyde, K.W., "Propeller Performance of Wright Brothers' 'Bent End' Propellers", submitted to the Journal of Aircraft, April 2000.

[3] "The Wright Stuff," Part IVc, WW I Aero Magazine, May 1993

[4] McFarland, M.W., *The Papers of Wilbur and Orville Wright, Including the Chanute-Wright Letters and Other Papers of Octave Chunute*, Arno Press, New York, Vol 2, 1906-1948

[5] "Aerodynamic Characteristics of Aerofoils I," NACA TR 93, 1921

[6] "Nomenclature for Aeronautics," NACA TR 240, 1927

[7] Von Mises, R., *Theory of Flight*,. McGraw-Hill, 1945

[8] Loukianoff, G.S., Z. Flugtech u. Motorluftschiffahrt, Vol 3, p 153, 1912

[9] Schlichting, H., "*Boundary Layer Theory*," 7th Ed., McGraw-Hill, 1979

[10] Anonymous, *The Unusual Records of the Stay-Tight Aeroplane Fabric*, Goodyear Tire and Rubber Co., Akron, OH, 1912

[11] Johnson, B.L., *Facility Description of the Walter H. Beech Memorial 7 X 10 Foot Low-Speed Wind Tunnel*, NIAR October 24, 1997, Revision A

[12] Barlow, J. B., Rae, W. H. and Pope, A., "*Low Speed Wind Tunnel Testing*," 3rd Ed., John Wiley and Sons, 1999

[13] Stainback, C.P. et al., "The Langley Research Center's Low-Turbulence Pressure Tunnel," AIAA 86-0762, 1986

[14] "Assessment of Wind Tunnel Data Uncertainty," AIAA standard, S-071-1999

[15] Abbott, I.H. and Von Doenhoff, A.E., *Theory of Wing Sections*, Dover, 1959

[16] McCormick, B.W., *Aerodynamics, Aeronautics, and Flight Mechanics*, John Wiley and Sons, 1995

[17] Selig, M.S. et al., "Experiments on Airfoils at Low Reynolds Numbers," AIAA 96-0062, 1996

[18] Ward, K.E., "Characteristics of an Airfoil as Affected by Fabric Sag, NACA TN 428, 1932

[19] Smith, A.M.O., "High Lift Aerodynamics," AIAA 74-939, 1974

Table 1 Surface Flow Visualization Summary

α	Bottom Surface
-4	reversal at LE to x/c=0.3 - 0.4
-3	reversal at LE to x/c=0.3 - 0.4
-2	reversal at LE to x/c=0.2 - 0.25
-1	reversal at LE to x/c=0.05 - 0.1
0	reversal at LE to x/c=0.05
1-14	all tufts attached
α	Top Surface
1	reversal at LE, fluttering TE
6.5	all tufts fluttering gently
8	pronounced fluttering entire upper surface
10	first tuft reversal at TE
14	entire surface shows reversal

Table 2 Uncertainty Analysis Summary

		Full-Scale			
a	**Bias**	**Precision**	**N**	**Mean**	**U**
	Drag Coefficient				
2	0.0004	0.0003	30	0.0100	0.0005
	Pitching Moment Coefficient				
2	0.0015	0.0057	23	-0.1610	0.0059
	Lift Coefficient				
2	0.0066	0.0141	20	0.8660	0.0156
		Third-Scale			
a	**Bias**	**Precision**	**N**	**Mean**	**U**
	Pitching Moment Coefficient				
0	0.0051	0.0016	58	-0.1445	0.0053
2	0.0051	0.0005	30	-0.1424	0.0052
7	0.0052	0.0007	5	-0.1180	0.0052
	Lift Coefficient				
0	0.0090	0.0141	20	0.6069	0.0167
2	0.0092	0.0021	30	0.8220	0.0094
7	0.0099	0.0066	5	1.2300	0.0119

Figure 1 Wright Model B Flyer (1910)

Figure 2 Plan View of the Wright Model B Flyer (one half shown)

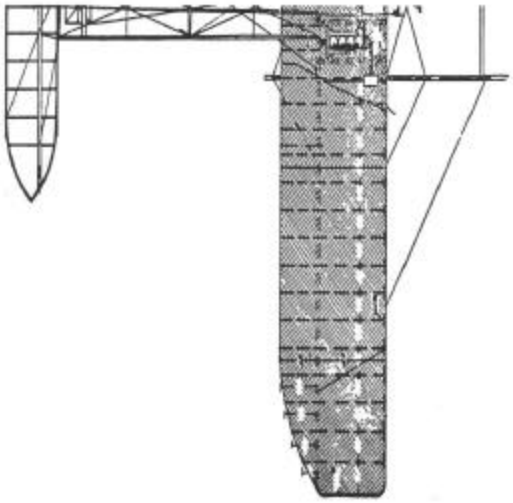

Figure 3 Model B Rib Showing Spar Locations and Angle-of-Attack Reference Line

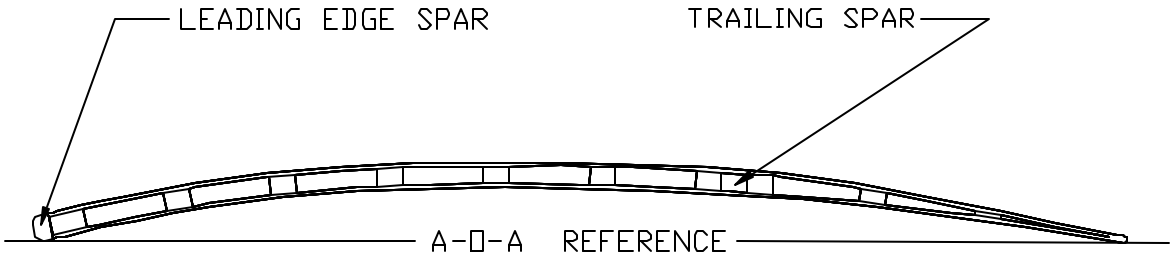

Figure 4 Comparison of Measured Rib Geometry to Airfoil II Model at the Airfoil Leading Edge

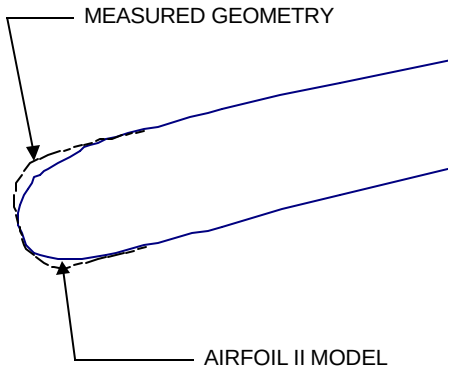

Figure 5 Reference Lift Data

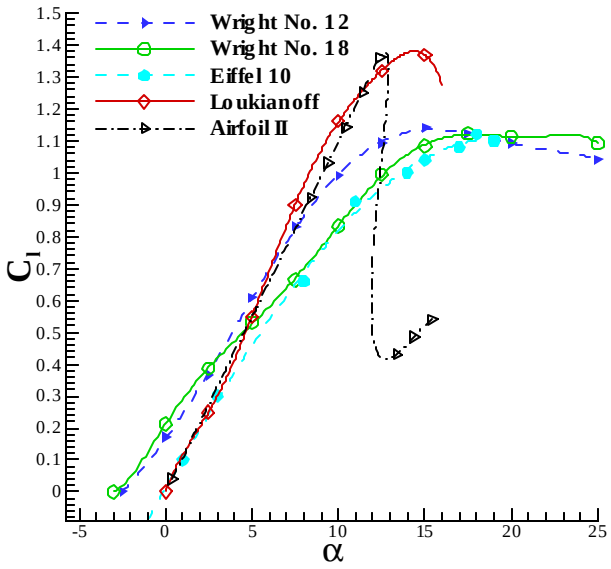

Figure 6 Sample of Airfoil II Predicted Pressure Distributions

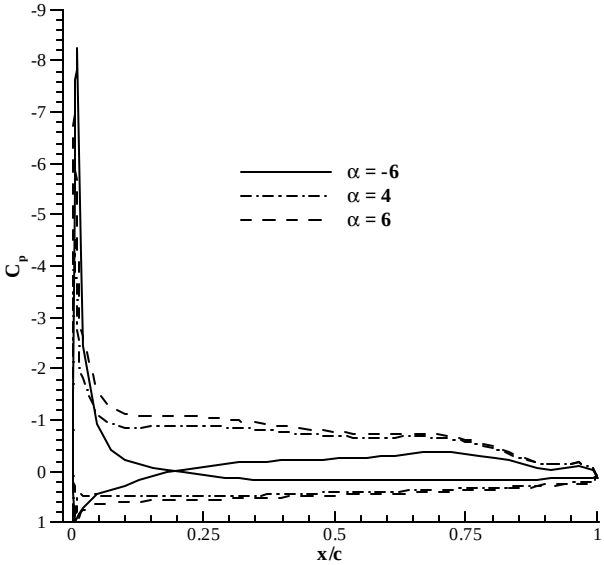

Figure 7 Full-Scale Model B Airfoil Model Design

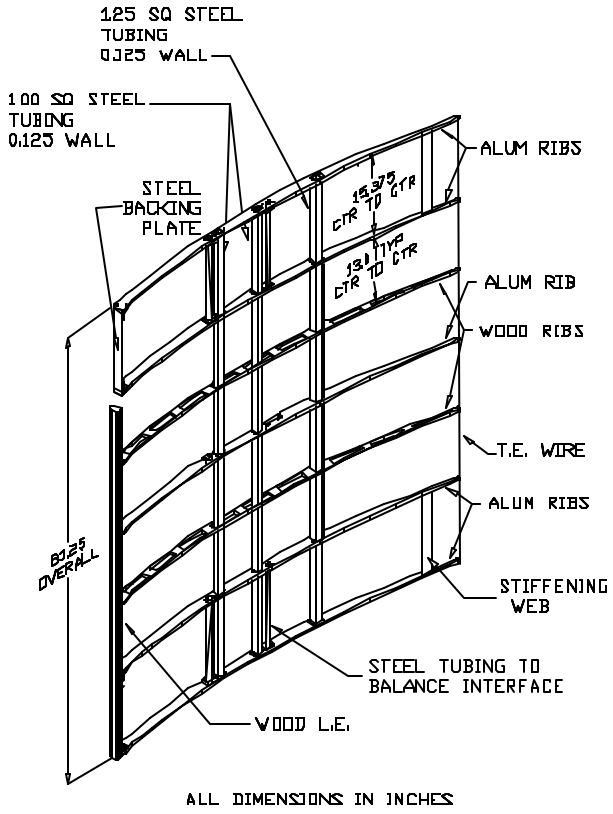

Figure 8 Full-Scale Model Under Construction

Figure 9 Third-Scale Model: Spars and End Ribs

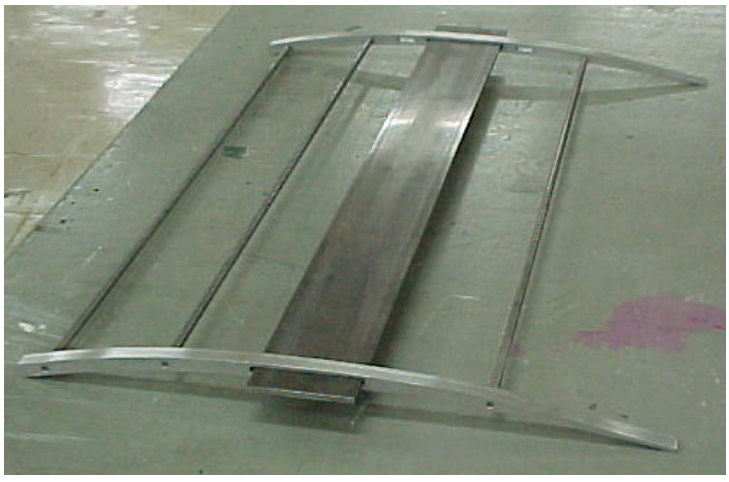

Figure 10 Third-Scale Model Construction: Routing Pressure Tubes

Figure 11 The Full-Scale Model Installed in the Walter H. Beech Memorial 7 X 10-Foot Low Speed Wind Tunnel at Wichita State University

Figure 12 The Third-Scale Model Installed in the NASA LaRC Low Turbulence Pressure Tunnel

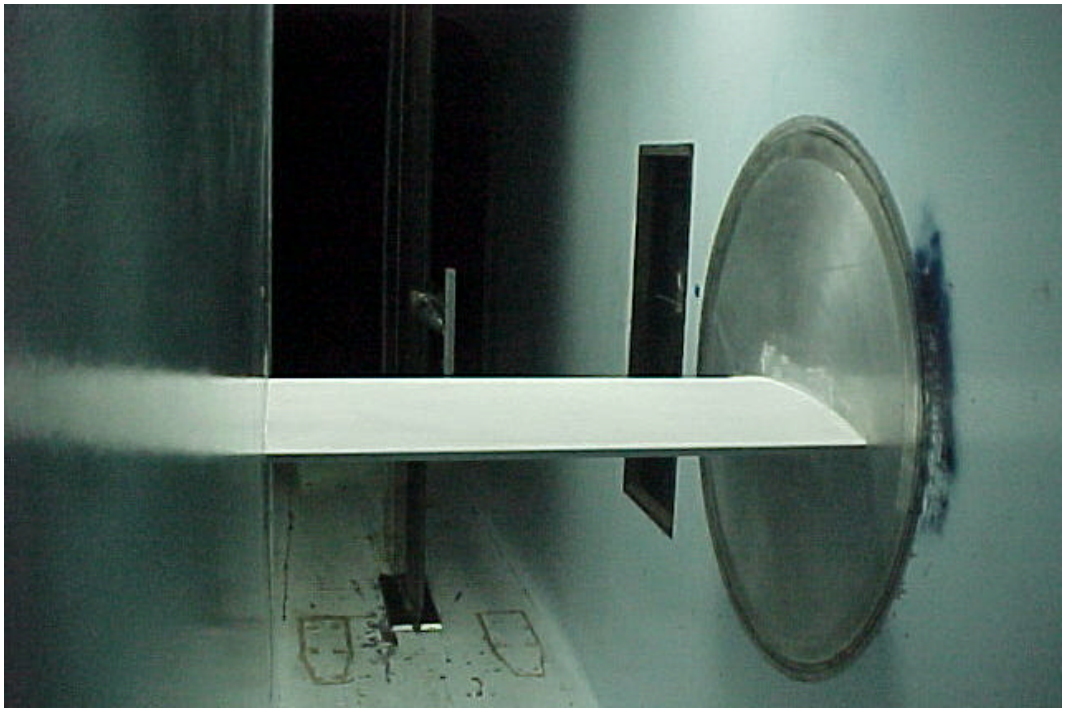

Figure 13 Sample Wake Data (Full-Scale)

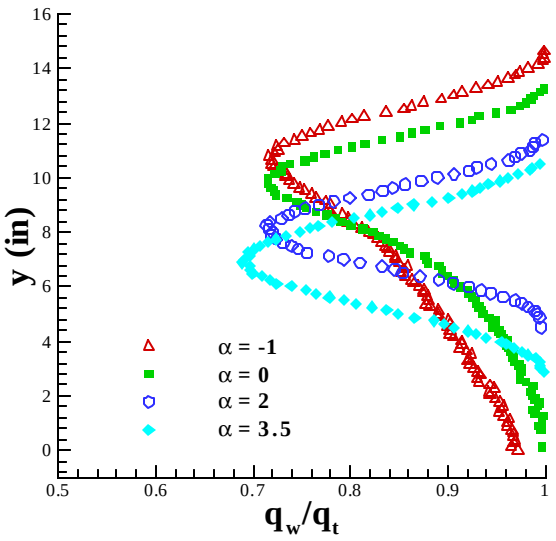

Figure 14 Drag Polar

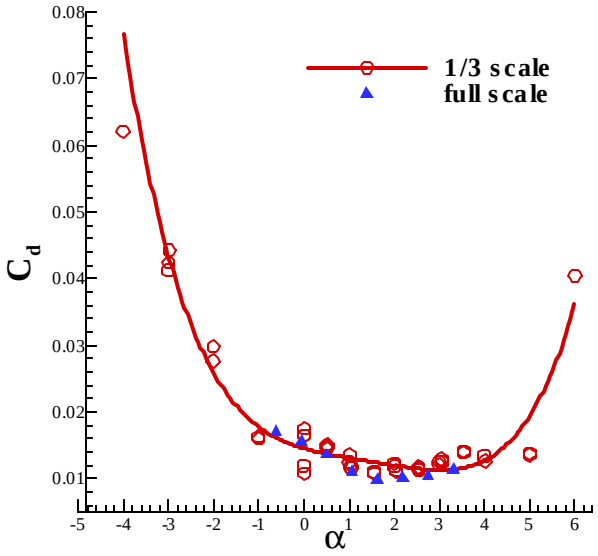

Figure 15 Pitching Moment Polar

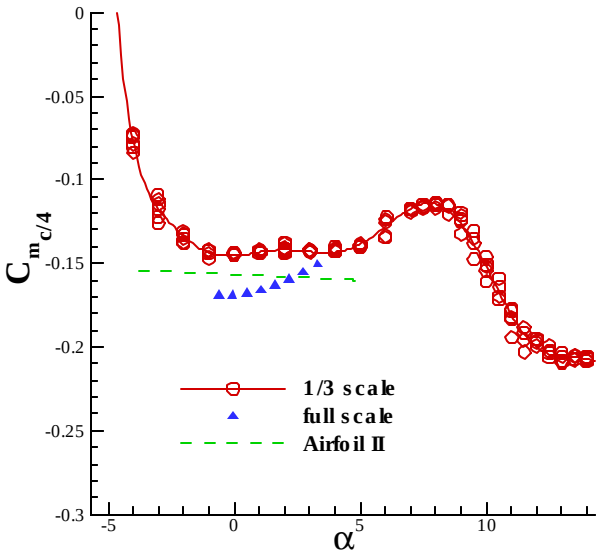

Figure 16 Lift Polar

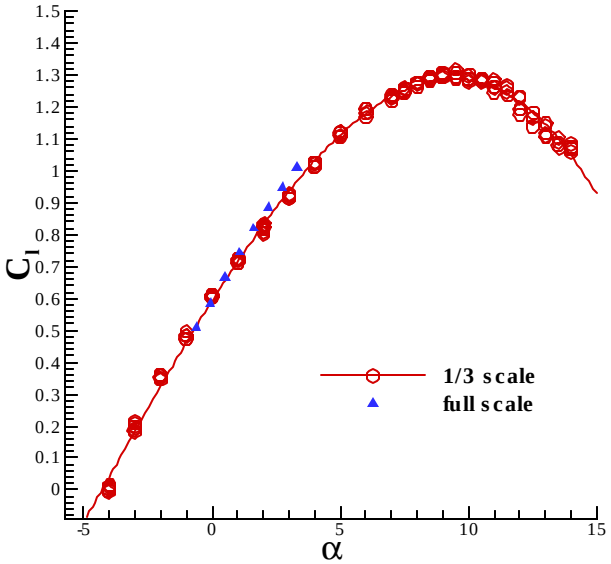

Figure 17 Pressure Distributions for α=-4° and α=0°

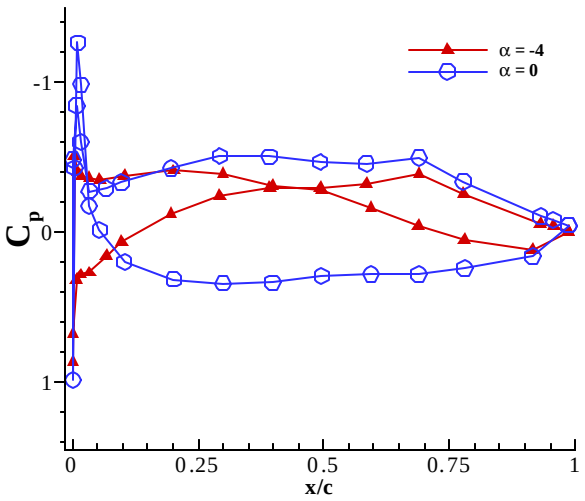

Figure 18 Pressure Distributions for α=4° and α=6°

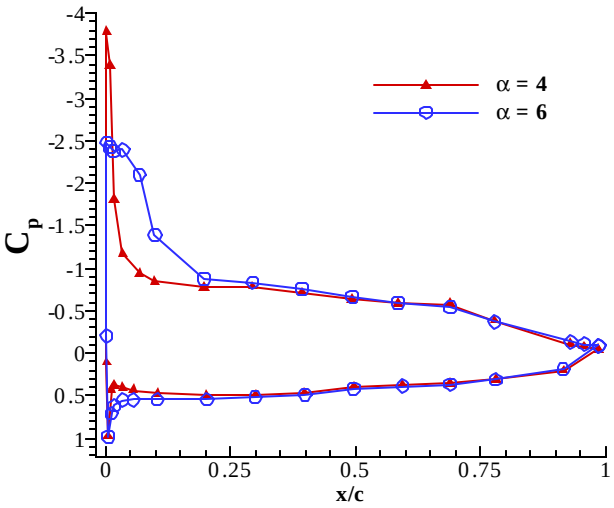

Figure 19 Pressure Distributions for α=8° and α=12°

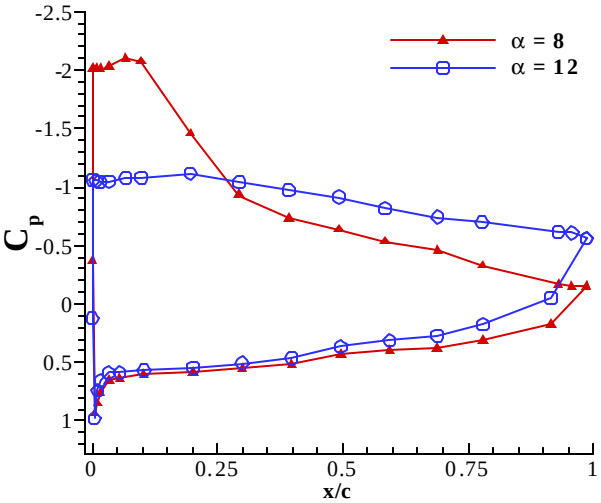

Figure 20 Effect of Upper Surface Fabric Deformation on Lift Polar